

Investigation of a Channeling High-Intensity Laser Beam in Underdense Plasmas

Z. Najmudin, A. E. Dangor, A. Modena, M. R. Salvati, C. E. Clayton, C. N. Danson, Daniel F. Gordon, C. Joshi, *Fellow, IEEE*, K. A. Marsh, V. Malka, Patrick Muggli, D. Neely, and F. N. Walsh

Abstract—The interaction of an intense short pulse laser ($>5 \times 10^{18} \text{ Wcm}^{-2}$) with underdense plasma was extensively studied. The beam is found to be highly susceptible to the forward Raman scattering instability. At sufficiently high growth rates, this can lead to wavebreaking with the resultant production of a high flux of accelerated electrons ($>10^{11}$ for $E > 2 \text{ MeV}$). Some electrons are found to be accelerated well above the dephasing energy, up to 94 MeV. Self-scattered images intimate the presence of high-intensity channels that extend more than 3.5 mm or 12 Rayleigh lengths. These filaments do not follow the axis of laser propagation, but are seen to be emitted within an $f/4$ cone centered around this axis. Spectra of the self-scattered light show that the main contribution of the scattering is *not* from light captured within these filaments. But there is evidence for self-phase modulation from effects such as ionization and relativistic self-focusing. However, no clear correlation is observed between channel length and the number or energies of accelerated electrons. Evidence for high intensities within the channels is given by small-angle Thomson scattering of the plasma wave generated therein. With this method, the intensity is found to be of the order of 10^{18} Wcm^{-2} greater than 12 Rayleigh lengths from focus.

Index Terms—Electromagnetic propagation in plasma media, electromagnetic scattering electron accelerators, plasma waves.

I. INTRODUCTION

THE advent of high-intensity short pulse laser systems has reignited interest in many possible applications of high-power lasers. The most noteworthy of these include the fast-igniter scheme for inertial-confinement fusion (ICF) [1], generation of coherent short wavelength radiation [2]–[4], and production of large amplitude plasma waves for next-generation particle accelerators [5]. The interactions are characterized by rapid ionization (through the large intrinsic electric field of the laser) [6], [7], susceptibility to instabilities (because of the increased intensity-dependent growth rates) [8], [9], and the non-

linear response to the laser of the plasma. The nonlinearity can manifest either through relativistic effects [10], [11] or through modification of the plasma via the ponderomotive force (or light pressure) of the extremely intense laser pulse [12]. An example of this is in the hole-boring creation of a guiding channel [13], which is of vital importance in the fast-igniter scheme.

Rapid ionization through optical field ionization (OFI) is particularly important for the generation of large amplitude plasma waves, because through the use of a uniform gaseous medium, we can create a plasma with an almost uniform initial density [14]. The plasma wave formed can thus be of constant (plasma) frequency. Such a medium is also ideal for the study of instabilities in this high-intensity regime, because it presents a long scale length over which the instability can grow [15]–[17], and allows us to distinguish the signatures of many different density regimes [18]. Particularly significant has been the first optical observation of the forward Raman scatter (FRS) instability [10], [19]. This four wave process generally has a smaller growth rate than does the three-wave Raman processes, which are possible off the axis of the laser propagation (i.e., the light is scattered out of the cone of the laser beam). Hence, until the use of high-intensity lasers, FRS was only significant at density close to the quarter-critical surface of laser–solid interaction [20]. With laser intensities that can routinely reach relativistic intensities (i.e., the quiver velocity of the electrons in the laser field is close to the speed of light), the growth rate of FRS is close to its maximum [9] and thus allows a laser pulse to exhibit FRS at much lower densities. FRS studies are difficult with long pulses (trying to offset the lower growth rate with a longer growth time), because on time scales $\gg 1$ -ps ion motion can destroy the favorable phase matching for FRS. FRS is particularly interesting, because the scattering process generates a large amplitude plasma wave that travels with the laser pulse at close to the speed of light. This plasma wave can be responsible for the acceleration to relativistic energies of trapped electrons from within the plasma [19]. This can have serious implications not only as a possible compact source of high-energy electrons, but also in ICF schemes in which the generation of such high-energy particles can have significance to the distribution of energy into the compressed fuel pellet.

The nonlinear optical properties of an underdense plasma when subjected to an intense laser pulse [21] can be as substantial as in solid–laser interaction. This is because a high-intensity laser pulse modifies the refractive index of the plasma as it travels through it. This can be achieved primarily in three ways, ionization [22], [23], plasma blow-out [24], [25], and relativistic effects [10], [26]. All three effects can modify the prop-

Manuscript received October, 2 1999; revised February 20, 2000. This work was supported by EPSRC, with the aid of EPSRC visiting fellowships.

Z. Najmudin, A. E. Dangor, A. Modena, and M. R. Salvati are with Blackett Laboratory, Imperial College, SW7 2BZ, London, U.K. (e-mail: zn1@ic.ac.uk).

C. E. Clayton, C. Joshi, and K. A. Marsh are with the Department of Electrical Engineering, University of California at Los Angeles, Los Angeles, CA 90095 USA.

C. N. Danson, D. Neely, and F. N. Walsh are with Central Laser Facility, Rutherford Appleton Laboratory, Chilton, Didcot, OX11 0QX Oxon, U.K.

D. F. Gordon is with the Naval Research Laboratory, Washington, DC 20375 USA.

V. Malka is with LULI, École Polytechnique-Université Pierre et Marie Curie, 91128 Palaiseau Cedex, France.

P. Muggli is with the Department of EE-Electrophysics, University of Southern California, Los Angeles, CA 90089 USA.

Publisher Item Identifier S 0093-3813(00)07242-8.

agation of the laser pulse, and they can result in spectral modification of the pulse. (All of the effects can be termed generally as manifestations of self-phase modulation of the laser beam.) Ionization, which tends to decrease the refractive index on axis, where intensity and, hence, OFI rates are highest, can act to defocus the laser beam. Plasma blow-out, which is caused by the transverse ponderomotive pressure of the intense laser pulse, and relativistic effects, which make the electrons quivering at velocities close to c seem more massive, increase the refractive index, hence, making the plasma act like an optical fiber. If the focusing caused by these two effects can overcome the natural diffraction of the laser beam, the laser beam waist will be reduced compared with its size were it focusing in vacuum. These two effects acting concurrently (because both occur naturally at high intensities in a plasma) are generally termed together as relativistic self-focusing [11], [27]. If the beam reaches such a size where the self-focusing effect is exactly balanced by natural diffraction, the beam can reach an equilibrium state, where it is said to be channeling. A simple treatment for a perfect Gaussian beam that only considers these two combined effects shows that channeling occurs at a critical laser power for relativistic self-focusing $P_{cr} \approx 17(\omega_0/\omega_p)^2$ GW. Indeed, if this threshold is exceeded, the beam size should be reduced. For nonideal beams, this threshold is weakly dependent on intensity [28]. Relativistic channeling has long been conjectured as a possible means of increasing the interaction length of plasma-based accelerator schemes and increasing the gain length of X-ray laser schemes, as well as providing the hole-boring path for the fast igniter concept.

This paper describes a series of experiments performed with the CPA:Vulcan laser [29], which provides 30 J in an 1-ps laser pulse at $1.054 \mu\text{m}$. When focused with an $f4.5$ focusing optic, it produces a four times diffraction limited spot of around $20\text{-}\mu\text{m}$ diameter. This corresponds to on-target intensities of up to $5 \times 10^{18} \text{ Wcm}^{-2}$. At such intensities, the normalized vector potential (which at low intensities is equal to the ratio of classic quiver velocity of the electrons in the laser field to the speed of light) is $a_0 \approx 2$. Hence, such a laser should be highly susceptible to the phenomena discussed above. The setup for the experiment is described in Section II. The results of the different diagnostics are detailed in Section III. In particular, emphasis is given to propagation, as measured by several forms of imaging, and to modulational instabilities of the laser pulse that give rise to fast electron production. We conclude with a summary in Section IV.

II. EXPERIMENT

The laser was focused onto the edge of a collimated flow of gas from a supersonic gas jet. The gas jet had been diagnosed previously by interferometric techniques [30], [48]. These measurements confirm a relatively uniform density profile over a range similar in size to the gas jet orifice. This type of nozzle is also characterized by a sharp gas–vacuum boundary ($\sim 500 \mu\text{m}$), which helps to minimize ionization-induced refraction of the laser pulse. The gas jet had backing pressures up to 100 bar of either He or H_2 , which gave plasma densities up to $5 \times 10^{19} \text{ cm}^{-3}$, over a distance of 3.5 mm, the bore size of the gas jet used in these experiments. The laser beam travels

in vacuum after being (grating) compressed [29] to 1 ps to the edge of the gas jet, to mitigate the pulse degradation that would result from the resulting high B-integral. For the same reason, the beam is focused with a ($f4.5$) reflective off-axis parabola.

The interaction is diagnosed in several ways. The transmitted beam is spectrally resolved to look for signs of FRS. The intensity of this transmitted light is reduced by allowing some of the light to leak through a pellicle with a high-reflection coating around $1 \mu\text{m}$. This is to ensure that the spectrum is not modified by self-phase modulation as it passes through the collection optics. The FRS spectrum is also used to ascertain the density of the interaction on each shot. This is possible because the FRS spectrum produces a satellite separated from ω_0 by ω_p ($\omega_s = \omega_0 \pm \omega_p$). Because the group velocity of the plasma wave off which the FRS scatters is relativistic, there is minimal thermal correction to the plasma frequency. So $\omega_p^2 = (n_e e^2 / \epsilon_0 m_e)$, where n_e is the electron plasma density. The density obtained in this way agrees well with double the number of neutrals obtained for the same gas jet backing pressure as obtained by interferometry (because both helium and hydrogen gases have two electrons per neutral). The error in the density obtained by this method is close to 6% over the whole density range considered here. The electron spectrum resulting from electrons trapped in the FRS-generated plasma wave is also recorded. Holes were made in the collection optics of the transmitted laser beam, so that both electron and laser spectra could be made simultaneously without unwelcome scattering of the electrons.

Direct evidence of the large amplitude plasma wave is obtained by small-angle collective Thomson scattering of a 527-nm probe beam. The probe beam of a size ($\approx 5 \text{ mm}$) sufficient to fully illuminate the whole plasma was injected nearly orthogonal (74°) to the direction of propagation of the driving CPA laser pulse. It was also orthogonal to the plane of polarization of the driver beam to minimize spurious signal from self-generated second harmonic, caused by relativistic Thomson scattering or density/intensity gradients within the plasma [31]. The Thomson scattered signal was taken at $3.5^\circ \pm 1.5^\circ$ to the probe beam (77.5° from the direction of propagation of the laser).

For proper wavematching, $\omega_s = \omega_0 - \omega_p$, and $\vec{k}_s = \vec{k}_0 - \vec{k}_p$, where the subscripts $s, 0$, and p refer to the scattered, incident and plasma wave. Because $\omega \approx ck$ for all of the waves in the case of a plane infinite relativistic plasma wave, scattering is only permissible in exactly the same direction as the incident laser [32], as shown in Fig. 1(a). However, in our experiment, the plasma wave is constrained to the order of $10 \mu\text{m}$ by the focal spot size of the laser. Hence, the relativistic plasma wave has a radial component to the wave vector comparable to k_p , because for $n_e = 1 \times 10^{19} \text{ cm}^{-3}$, λ_p is also around $10 \mu\text{m}$. This allows resonant Thomson scattering off-axis, as is shown in Fig. 1(b). By focusing the probe and the scattered beams, it is possible to spatially isolate the undeviated probe beam and to dump its energy on a razor blade, reducing spurious light from this unscattered component. The scattered light is then reimaged onto the slit of an imaging spectrometer, providing a spatially resolved profile of the plasma wave, along the direction of the driver beam.

To complete the diagnostics, there are three imaging channels, one schlieren and two imaging self-scatter of the driving beam. The schlieren channel provides information about the

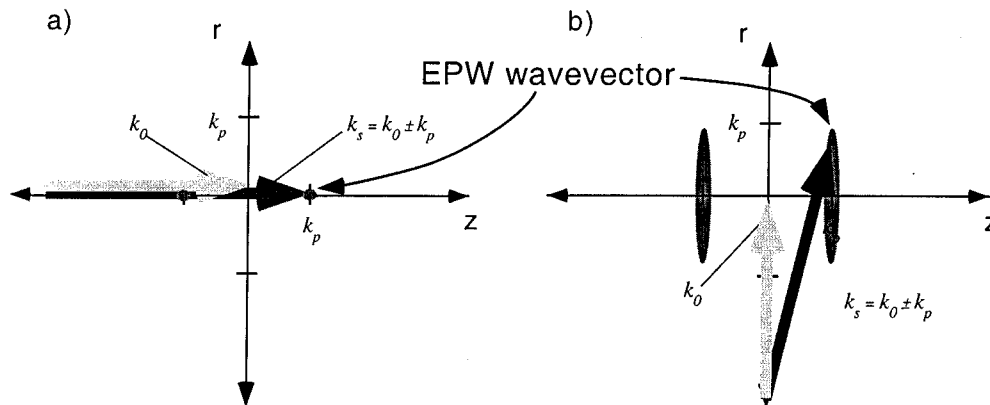


Fig. 1. Thomson scattering k -vector matching (a) for infinite plane waves (with k -vector $\pm k_p$) wavematching is only valid in the exact forward direction from the fast wave $k_p \approx \omega_p/c$. (b) For a plasma wave constrained to a focal spot on the order of the plasma wave length, the wave has a spread in radial k vector $\approx k_p$, which allows direct scattering off this fast wave at greater angles, allowing spatial monitoring of the wave.

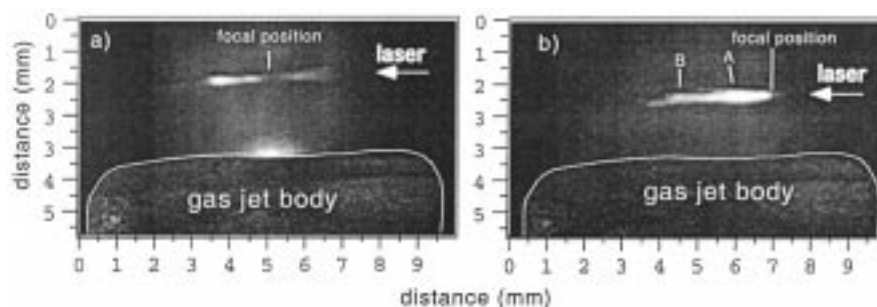


Fig. 2. Images showing self-Thomson scattered images of propagation of a 25-TW laser in underdense plasma, when focused (a) at the center of the jet (orifice size = 3.5 mm), and (b) 0.5 mm from the edge of the jet. Direction of the laser is right to left, and the extent of the gas is marked by the faint (time-integrated) background glow of the unionised. A and B indicate branching of the filaments.

density channels within the plasma by reimaging light refracted by these density channels. This is done by putting a wire stop at a virtual focus of the probe beam (which has been previously split from the small-angle Thomson scattering signal), so that only those rays deviated by density gradients may pass the stop. The self-scattering imaging channels were placed; one at 30° to the incident laser in the plane of polarization of the laser, and the other orthogonal to both drive laser and its polarization. For the imaging channel at 30° , a transmission grating of spacing 2 l/mm was placed in the beam at a point where the beam was collimated, in order to give a spectrally resolved image away from the (zero-order) transmitted image. The self-scattered light orthogonal to the plane of polarization was also spectrally resolved. However, in this case, the image was split with a beam splitter, and reimaged onto the slit of a standard high dispersion spectrometer/charge-coupled device (CCD) system.

III. RESULTS

A. Imaging of Self-Scattering

Two images are presented in Fig. 2, for 25 TW focused either at the center or the edge of the jet. The resolution of these images is limited to $45 \mu\text{m}$ by the pixel size of the CCD cameras used. Both show a beam diverging away from focus in roughly the expected cone angle ($f4.5 \approx 16^\circ$). The image with the focus at the center of the jet shows plasma over the whole length of the jet, 1.75 mm either side of focus. At this edge of the gas jet, the

expected intensity in vacuum would be $\approx 1 \times 10^{16} \text{ Wcm}^{-2}$, just above the threshold value for double ionization of helium, the gas used for these shots. Also note that the image shows a minimum in scattering intensity close to focus. This (as explained by Gibbon *et al.* [33]) is because of volumetric effects; simply, there are fewer scatterers at focus because of the small focal spot size. The image with the focus at the edge of the jet also shows Thomson scattered light over the whole length of the gas jet. However, in this case, the other edge is now 3.5 mm from focus, where the expected vacuum intensity would be $2.5 \times 10^{15} \text{ Wcm}^{-2}$. Though this is sufficient to singly ionize helium, it is below the OFI threshold required for full ionization of He atoms. It is therefore surprising that the scattering intensity does not show a marked diminution at this distance from focus.

The spectrum of the transmitted beam (Fig. 3) is also significantly different, even though in both cases, the beam is unstable to FRS. When focused at the center of the jet, the spectra shows narrow satellites sat on top of a spectrally wide, blue-shifted shoulder of the original laser frequency. When focused at the edge of the jet, though, the anti-Stokes lines of the Raman spectra become much broader and often display modulations of the satellite. The blue-shifted shoulder is greatly reduced. (Note in both cases the longer wavelength Stokes satellite cannot be seen clearly because of the reduced efficiency of the silicon-based detector used. The fact that the Stokes signal is observed at all when focusing at the edge of the jet is presumably because of its greater spectral width.) The greater width and modulations

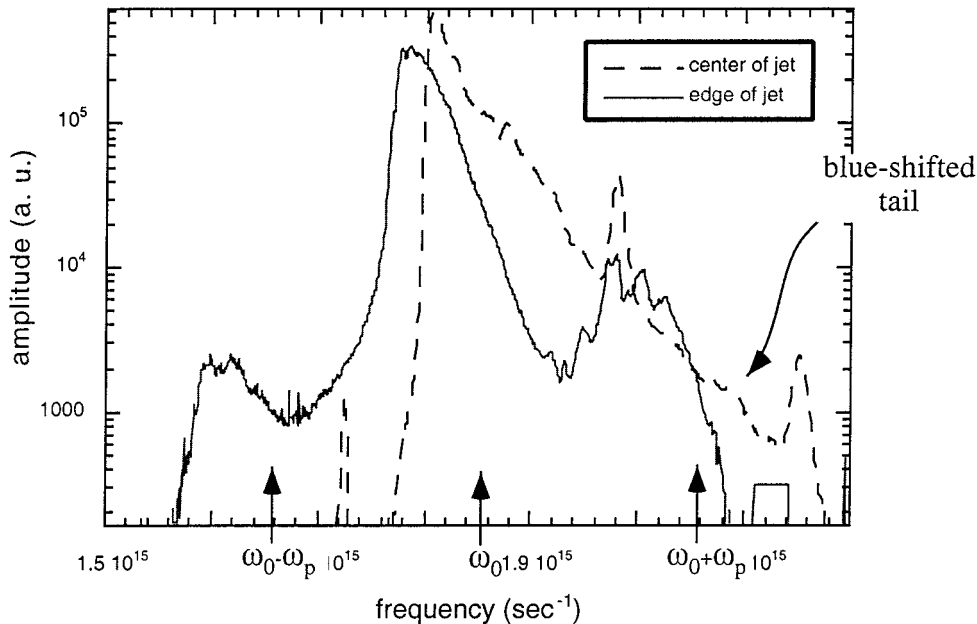


Fig. 3. Two transmitted light spectra for a 25-TW laser beam focused in helium, creating an underdense plasma of density $1.3 \times 10^{19} \text{ cm}^{-3}$, one with the focus at the center of a 3.5-mm gas jet, and the other at the edge of the jet.

of the satellite, with the focus at the edge of the jet, point to wavebreaking of the Raman-induced plasma wave and, hence, indicate a greater growth rate for FRS [10]. This manifests in the electron spectra, which in this case register electrons accelerated up to $50.7 (\pm 1.8)$ MeV because of the wavebreaking. However, when focused at the center of the jet, no electrons are detected above 20 MeV.

These results are not surprising when we consider the density n_e at which ionization-induced refraction becomes important, for light of wavelength λ (and critical density n_{cr}) is given by $n_e/n_{cr} > \lambda/z_r$. We can calculate the Rayleigh length, defined as twice the length over which the laser intensity drops by a factor of 2, using the simple expression $z_r = 2\sqrt{2}fd$, where f is the f -number of the focusing optics and d is the focal spot diameter. The expression comes from purely geometrical assumptions and is reasonable for nondiffraction-limited laser beams. Taking $f = 4.5$ and $d = 20 \mu\text{m}$, the Rayleigh length in our condition is $z_r = 260 \mu\text{m}$. For $\lambda = 1 \mu\text{m}$ light, we find that ionization-induced defocusing becomes important for $n_e \approx 4 \times 10^{18} \text{ cm}^{-3}$. Above this density, we can expect that the maximum vacuum intensity will not be reached. This is indeed apparent in the Raman spectra with the focus at the center of the jet, where the anti-Stokes amplitude actually decreases above this density. In fact, at a density of only $1.8 \times 10^{19} \text{ cm}^{-3}$, the Raman satellites are completely “washed out” by the rising blue-shifted tail of the driver frequency. The blueshift is generated by ionization and the resultant time-dependent decrease in refractive index, similar to the spatial dependence, which causes ionization-induced defocusing. Hence, it is a good indicator of the importance of ionization in the interaction [23]. The Raman spectra, when focused at the edge of the jet, exhibits a greatly reduced ionization blue-shift, and so indicates an alleviation of ionization-induced diffraction effects. This shows the importance of good positioning of the focal position. Indeed, we find

that movements as small as $250 \mu\text{m}$ either side of an optimum position can reduce the maximum number of accelerated electron by orders of magnitude. This also demonstrates the importance of having a (supersonic) gas jet with a sharp vacuum–gas interface.

Also interesting to note in Fig. 2(b), which shows an image with the focus at the edge of the jet, is that the filament not only propagates forward, but also has filament branching away from the main filament, marked in the figure as A. Indeed, the main filament seems to terminate into two filaments moving away at an angle of around 10° , at position B. This lateral movement of laser energy, which does not necessarily occur from the initial focal position, was seen often when the beam shows signs of channeling. Simulations of channeled beams (with slightly different parameters) have shown such lateral movement can result from the termination of transverse oscillations of the beam center because of “hosing instabilities” [34], [35]. In these simulations, it is seen that this lateral filamentation can be seeded by kinking of the electron beams generated by the interaction, which are subject to transverse center of beam instabilities. Sideways motion of a high-intensity beam would of course have serious implications for applications of whole beam self-channeling.

Figs. 4 and 5 show a series of images of shots taken with fixed density and increasing intensity (Fig. 4), and with fixed intensity and increasing density (Fig. 5). The ratio of laser power over critical power for self-focusing P/P_{cr} is presented for each shot, which is proportional to laser power/electron density. In all cases, the laser was focused at the same position, $500 \mu\text{m}$ from the edge of the gas jet (i.e., $x = 4.75 \text{ mm}$ in the figures). As we can see for a fixed plasma density of $1.4 \times 10^{19} \text{ cm}^{-3}$, as the laser power is increased, the length of the scattered signal increases. Indeed, at a laser energy of 4.6 J ($P/P_{cr} = 3.8$ —for which $a_0 \approx 1$), we see intense scattering only near

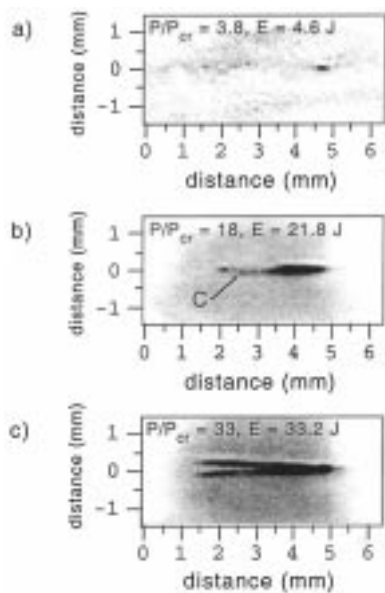


Fig. 4. Self-scattered images of laser propagating in a gas jet at a plasma density of $1.4 \times 10^{19} \text{ cm}^{-3}$, for increasing on target laser energy and correspondingly P/P_{cr} . Direction of the laser is right to left, and the extent of the gas is marked by the faint (time-integrated) background glow of the ionized gas. C indicates the branching of a filament.

focus [Fig. 4(a)]. With increasing energy, the scattering region increases, in a volume closely representing the $f4$ cone of the laser beam, until the laser energy is about 15 J, where the length of this cone no longer increases. However, signs of a thinner region of scattering extending away from this cone are apparent [e.g., the filament marked C in Fig. 4(b)]. For P/P_{cr} around 15, this filament extends by over 2 mm; all the way to the other edge of the gas jet, as seen in Fig. 4(b). As mentioned before, to maintain intensities above the ionization threshold, for the first ionization of helium, the intensity must be greater than $2.5 \times 10^{15} \text{ Wcm}^{-2}$. In reality, the intensity in these filaments must be rather higher, not only because we do not see any Thomson scattered signal for beam energies less than 3 J, but also because we must be close to relativistic intensities to be subject to the plasma nonlinearities that cause these extended filament [36]. The laser power in the filament must be above P_{cr} . Because the original power of the laser beam is many times P_{cr} , this is not unreasonable. However, the fact that it takes powers many times P_{cr} to see these extended filaments suggest that much of the laser energy is not trapped into a long filament, as is evidenced by the ($f4$) cone of scattered light naturally diffracting away from the vacuum focal position. Fig. 4(b) shows the filament branching into two close to its end, as in Fig. 2(b), (marked C in the figure). This branching is even more apparent in Fig. 4(c), which shows two clearly separated filaments, both of high-intensity, propagating all the way from close to focus to the other edge of the jet. Many such instances of these multiple filaments are observed at $P/P_{cr} > 20$, though most tend to remain within the cone angle of the original laser beam.

Fig. 5 shows the Thomson scattered images for a variety of densities (again represented as a function of P/P_{cr}), for a fixed laser power of around 25 TW. Generally, the features are similar to those at corresponding values of P/P_{cr} for fixed density and

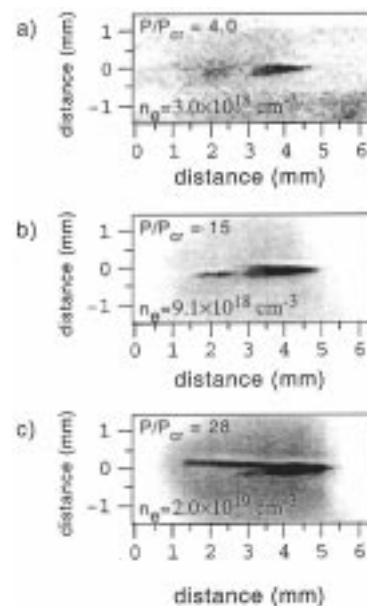


Fig. 5. Self-scattered images of propagation of a 25-TW laser in various densities of gas jet. Direction of the laser is right to left, and the extent of the gas is marked by the faint (time-integrated) background glow of the ionized gas.

increasing intensity (Fig. 4). In particular for $P/P_{cr} \approx 10$ –15, a clear filament can be observed, extending beyond a broader conical region of emission, where the laser appears to be diffracting naturally. At yet higher densities (and, therefore, P/P_{cr}), multiple filaments are again seen to form that can extend over the whole length of the gas jet. However, a major difference is observed at lower densities, i.e., closer to the critical power for relativistic self-focusing. Though the first sign of scattering is roughly at the same value of P/P_{cr} , the shape of the scattering region is different to that at low intensity. At low densities [Fig. 5(a)], we still see the conical shape of the laser beam diffracting naturally. However, with the equivalent P/P_{cr} at lower energy and higher density [Fig. 4(a)], we see a more intense, but much shorter scattering region. The difference in intensity of scattering is expected, because of the $n_e^2 \cdot I$ dependence of Thomson scattering. The difference in length of the scattering signals can be explained by the rate of ionization, which is different in the two cases. Because the intensities are well above the threshold values for tunnel ionization, the ionization rates and, hence, rate of ionization-induced defocusing is almost independent of the laser intensity. However, it does depend linearly on the density of plasma created, because the path difference between two rays traveling in ionized and nonionized parts of the jet is proportional to $\Delta n_e \cdot \partial l$. Therefore, at higher density, ionization defocusing can reduce significantly the distance over which the beam defocuses, as we appear to observe in Fig. 4(a). It also explains why it is necessary to be many times the critical power for relativistic self-focusing for us to see signs of self-channeling. As a result of the relatively high densities required in the self-modulated wakefield, as in our experiments ($>1 \times 10^{19} \text{ cm}^{-3}$), it is difficult to envisage channeling in such a scheme at powers close to P_{cr} , without the aid of a plasma-producing prepulse.

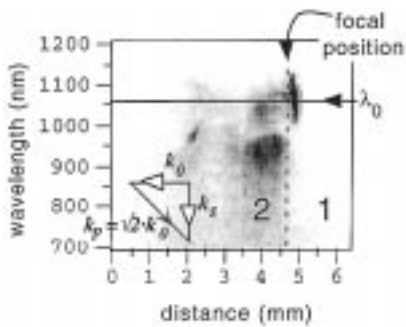


Fig. 6. Spectrally dispersed self-scattered images of propagation of a 33-TW $1.054\text{-}\mu\text{m}$ laser in plasma of density $1.4 \times 10^{19}\text{ cm}^{-3}$ (orifice size = 3.5 mm), viewed orthogonally to the direction of propagation. The laser travels from right to left and is focused at the marked position where $x = 4.75\text{ mm}$. Inset shows the wavevector matching for this angle of scattering.

B. Spectra of Self-Scattered Images

Most studies of self-channeling of laser pulses have relied on the Thomson scattering images to infer propagation lengths of the interaction. However, despite the large amount of qualitative data we can obtain from these images, we must be wary in interpreting these images, as is demonstrated by spectral dispersion of these images. Fig. 6 shows a typical spectrum of one of the Thomson scattered images, taken with a transmission grating placed in front of the image forming lens, so that there is combined spatial and spectral information. The image was taken at $P/P_{cr} \approx 30$; (density = $1.4 \times 10^{19}\text{ cm}^{-3}$, laser power = 33 TW). The figure shows some surprising features. Firstly, in the region marked 2 in the figure, the spectra shows a prominent blue satellite. A similar feature to the red side is not seen, because of the insensitivity of the Si-based CCD camera used, above $1.1\text{ }\mu\text{m}$. For Thomson scattering to be in this collective regime with clearly separated satellites, the relation $k_p \lambda_d < 1$ must hold. In the case of viewing orthogonal to the laser propagation, $k_p \approx \sqrt{2}k_0$, as shown in the inset of Fig. 6. This would suggest that the temperature of the scattering plasma is less than 3.5 keV. Indeed, the satellite, just beyond the focus, shows no discernible Bohm–Gross shift to the plasma frequency ($\omega_{BG}^2 = \omega_p^2 + v_{th}^2 k^2$), suggesting that it is much colder than this. The Thomson scattering nature of this light is confirmed by variations in density or intensity, which show the scattering is proportional to $n_e^2 \cdot I$, as expected in the collective regime. Noticeably, this blue satellite appears to start slightly beyond the focal position, and its length is the same as that of the bright cone of naturally unchanneled light seen in Figs. 4 and 5. Indeed, it is difficult to view the scattered light from the longer length filaments because the scattering is much dimmer, except close to where they terminate, where they show the same behavior as for the uncaptured light closer to the vacuum focal position [for example, as in Figs. 4(b) and 5(b)].

As can be seen, the satellite shows a marked shift to the blue further into the gas jet. This second “burst” of scattering has a Bohm–Gross shift that corresponds to a temperature of around 450 eV. Also of interest is the ion feature; the scattering close to the wavelength of the driver pulse λ_0 , in particular, at the highest powers (or highest density because the spectra are similar for similar values of P/P_{cr}). As we can clearly see, this

feature seems to blue shift as the scattering comes from later in the propagation of the pulse. This blue-shifting could well be the result of ionization-induced self-phase modulation of the driver pulse. However, it is surprising that all of the scattered light becomes blue-shifted (without any λ_0 component), considering that most of the light at λ_0 detected in the forward scatter is unshifted (despite a strong blue-shifted tail from ionization). Recent higher resolution probing of this interaction [37] has showed that though much of the laser light is captured into a channel of a high f -number, a good amount of light leaks away from this cone, perhaps because of ionization-induced refraction [38] early in the pulse, or intense Raman side scatter [15], [16]. This light would then be subject to further ionization (because it travels through as yet nonionized gas), and further blueshifting. This simple picture could be complicated by the bulk motion of the plasma.

Another interesting feature is the broad bright burst of scattering centered on λ_0 , right at the start of the scattering region (marked 1 in the figure). The position of this scattering in the gas jet does not change and is very close to where we expect the vacuum focus position to be. The scattering only appears at the highest powers or densities (i.e., for $P/P_{cr} > 30$). Noticeably, it begins about 200–300 μm before the electron feature. The $1/e$ width of this feature is found to be $50.5 (\pm 1.0)\text{ nm}$, which corresponds to an electron temperature of around 350 eV, were this from incoherent Thomson scattering. But for any form of heavily damped scattering, we can expect that $k_p \lambda_d > 1$. This gives an upper bound for the plasma density in *this* region of $n_e < 1.3 \times 10^{18}\text{ cm}^{-3}$, suggesting that we are seeing scattering from close to the vacuum–gas interface. The sharp appearance of this scattering indicates that some form of stimulated process is involved; otherwise, incoherent scattering should scale with density and laser intensity and should be proportional in scattering intensity to the strength of the rest of the scattered signal (at least in changes of density and intensity). This type of scattering, where the plasma waves are heavily damped, is often referred to as stimulated Compton scattering. This demonstrates that self-scattering in these high-intensity interactions can be from different regimes, in different parts of the interaction, and is not necessarily Thomson scattering. It seems, therefore, that we must take great care in defining the properties of a self-channeling beam from only the images of scattered light.

C. High-Resolution Self-Scattering Spectra

Thomson scattered images were also obtained orthogonal to both the beam and the plane of polarization. This is the direction in which the scattering should be maximized. The images seen were qualitatively the same as those taken slightly off the plane of polarization, shown in Figs. 2, 4, and 5. Again, these images were spectrally dispersed. This was done by imaging the Thomson scattered light on to the slit of an imaging spectrometer, thus, giving higher spectral resolution, coupled to the spatial information. The slit was aligned along the direction of propagation of the laser. Fig. 7 shows a density scan of these spatially resolved spectra, for a variety of P/P_{cr} . Again, a series done with varying intensity are qualitatively similar, for the corresponding value of P/P_{cr} , except at the low intensity, where

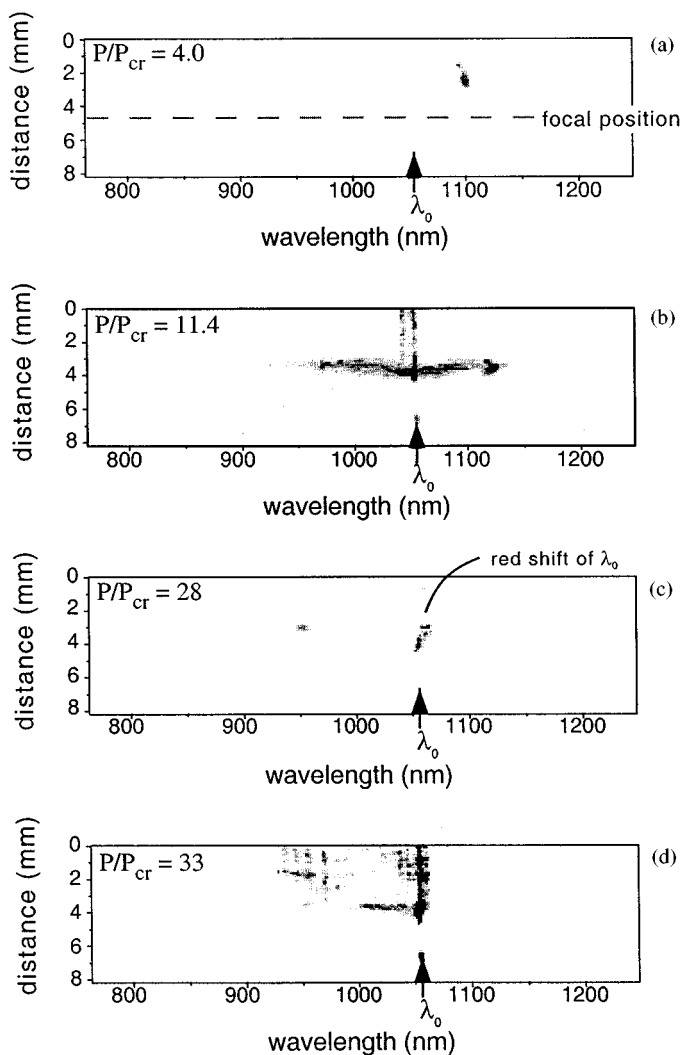


Fig. 7. Spatially resolved high-resolution Thomson scattering spectra in direction mutually orthogonal to direction of propagation of laser beam and its polarization for varying P/P_{cr} : (a) $P/P_{cr} = 4.0$ ($n_e = 3.0 \times 10^{18} \text{ cm}^{-3}$, $E_{las} = 27.2 \text{ J}$), (b) $P/P_{cr} = 11.4$ ($n_e = 7.5 \times 10^{18} \text{ cm}^{-3}$, $E_{las} = 30.9 \text{ J}$), (c) $P/P_{cr} = 28$ ($n_e = 2.0 \times 10^{19} \text{ cm}^{-3}$, $E_{las} = 27.6 \text{ J}$), (d) $P/P_{cr} = 33$ ($n_e = 1.4 \times 10^{19} \text{ cm}^{-3}$, $E_{las} = 33.2 \text{ J}$). Direction of the laser is upward. The focus is the same at $x = 4.75 \text{ mm}$ on the spatial axis.

the feature is smaller, because of ionization defocusing. For the lowest density case [Fig. 7(a)], the feature seems to have moved further along the direction of propagation of the laser (by over 1.5 mm). This gradual moving of the scattering feature away from focus as the density is reduced is seen in all of the Thomson scatter diagnostics. This indicates that ponderomotive reduction of the plasma density close to focus is more significant at the lowest densities. This is as expected because the space-charge restoring force will be less in this case. Noticeably, for all shots of low P/P_{cr} , there is an absence of the blue satellite, but the red satellite is clearly visible. This would suggest that in these shots, a three-wave stimulated scattering process was in action. However, for increasing density, the blue satellite does appear, as shown by the almost symmetrical feature in Fig. 7(b). The scattering, hence, appears to mirror the FRS (as we shall see later). Unfortunately, once more the Stokes (red) satellite is lost at densities greater than $1 \times 10^{19} \text{ cm}^{-3}$, because of the detector

response. On some, though not all, shots, at high P/P_{cr} , the scattering feature is seen to extend all the way to the edge of the jet [as shown in Fig. 7(d)]. The scattering then shows a preference for the blue side of λ_0 , as seen in the other imaging channels. However, the higher dispersion shows a curious feature, the presence of strong modulations in the broad-shifted blue satellite. The modulations are neither regular nor related to characteristic oscillations of the interaction. Strong modulation of ionization-induced blue-shifted light [39] has been observed previously, and it could be that it is just this blue-shifted light that is being rescattered. This extended modulated feature is not seen on all shots [e.g., Fig. 7(c)], because it depends on the angle of the filament created on the shot and, hence, is not seen when the filament is misaligned from the ($200 \mu\text{m}$) slit of the spectrometer used.

There is scattered light close to λ_0 along the whole length of the scattered signal in Fig. 7(d). This is in contrast to the scattering profile in Fig. 6, which showed only light to the blue side of λ_0 . Noticeably, the λ_0 light is slightly shifted close to focus, but this time to the red. This is clearer on Fig. 7(c), where there is no light from the filament passing into the spectrometer, and a shift of approximately 10 nm is observed. Such a shift could result from any process that acts to rapidly increase the refractive index of the laser beam as it travels through the gas jet. A simple estimate gives the wavelength shift of the fundamental frequency λ_0 as $\Delta\lambda/\lambda_0 = -L/2n_e w_p^2/w_0^2 d/dt(n_e/\gamma)$, where L is the interaction length, and the Lorentz factor γ , given in terms of the normalized vector potential, is $\gamma = (1 + a_0^2/2)^{1/2}$. Red shifts can result from processes that act to decrease the effective plasma density n_e/γ , such as relativistic or ponderomotive blow-out effects. From the shape of the red-shifting in Fig. 7(c), which takes place gradually as the light travels close to 1 mm in the gas jet, we can see that the red-shifting takes place on the time scale that it takes the pulse to traverse this distance. Calculating the change in density required over this distance to obtain such a shift, we obtain $\Delta(n_e/\gamma) \approx n_e$. If only density changes were responsible for this change, this would imply total cavitation of the plasma. This seems unlikely because we would then expect a rapid decrease in the strength of the signal as the number of scatterers is reduced. Indeed, simulations show that the hot plasma temperatures within self-focusing filaments serve to prevent total cavitation [41]. Hence, the focal spot size must also be changing, giving evidence of an increase in intensity within the filaments.

The plasma channels left behind by the filaments are clearly observed by schlieren images of the plasma, which serve to highlight high-density gradients caused by ionization of the laser channels, by ponderomotive expulsion, and by thermal expansion of the plasma. A particularly long and straight channel extending over the whole length of the gas jet is shown in Fig. 8.

D. Small Angle Resonant Thomson Scattering

As described before, a frequency-doubled probe beam was injected to the CPA driver at 74° . The scattering of this probe beam at an angle of 3.5° has a component corresponding to the scattering from a wave whose wavenumber k_p is equal to that of

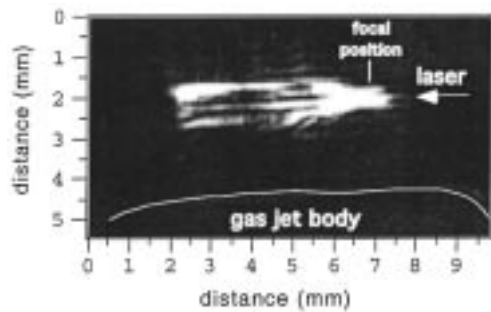


Fig. 8. Schlieren image delineating sharp density gradients in a plasma created by propagation of a 29-TW laser in a gas jet, giving a plasma density of $n_e = 1.4 \times 10^{19} \text{ cm}^{-3}$. Direction of the laser is right to left.

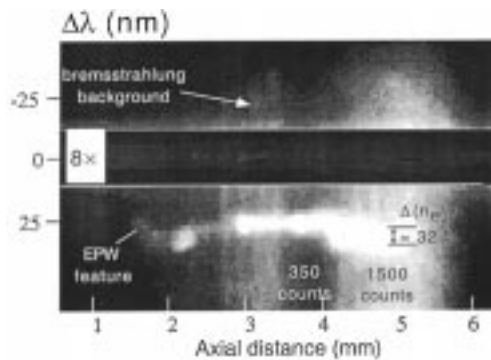


Fig. 9. Small-angle Thomson scattering image of an electron plasma wave (EPW), generated by a 28-TW beam in a plasma of density $1.9 \times 10^{19} \text{ cm}^{-3}$. The laser travels from right to left (and is focused at $x = 4.75 \text{ mm}$). Spurious scattered light at 527 nm has been attenuated to emphasize the ω_p shifted light caused by the EPW. The spectrally broadbands of background light are from bremsstrahlung radiation.

the FRS-generated “fast” plasma wave. Fig. 9 shows this light that has been reimaged at the slit of an imaging spectrometer. The resulting image is gated with a gated-optical imager with a gate time of 1 ns. Without the gating, the scattering signal would be obscured by recombination lines of helium in this part of the spectrum. The horizontal direction, therefore, gives spatial information, whereas the vertical is spectral. A bright feature is seen at the wavelength of the probe (527 nm). This is despite the presence of a notch filter, which attenuates this light by 10^2 . This is mostly stray scattering from the optics used, as can be seen by the uniformity of this signal across the whole field. We do not expect to see much scattering from ion wave-type oscillations because the phase velocity of the waves detected at this angle would be too high. The feature below, shifted by $\approx 30 \text{ nm}$, is the collective scattering from the electron plasma wave ($\omega_s = \omega_0 - \omega_p$). Notice that no corresponding feature is observed to the blue side of 2ω , because it is prohibited by the wavematching conditions. The scattering has a bursting nature (i.e., strongly modulated in intensity), similar to some of the self-scattered images of the driver beam. The signal on this shot is particularly impressive because it extends over the whole length of the gas jet, 3.5 mm or more than 12 Rayleigh lengths from focus. Indeed, we can detect the profile of the gas jet, with a dip in density in the middle and sharply falling density at the edges of the gas jet. The lower plasma frequency at the center of the gas jet caused by lower gas density was confirmed by taking

lower intensity shots focused at the center of the jet. These shots reproduce the lower density in their FRS spectra, and so exclude the effect of nonlinear processes, such as a relativistic or ponderomotive reduction in the effective plasma frequency. Indeed, the FRS spectra on the same shot as Fig. 9 has two anti-Stokes satellites at the two frequencies corresponding to the two different density regions of the jet. A limit for the extent of cavitation can be obtained by looking at the width of the scattered satellite near focus in Fig. 9. It is found to be about 12.5 nm or about 33% of ω_p . So the reduction in density is not more than $\approx 50\%$. At the other edge of the jet, the satellite is even narrower, so that cavitation is even less significant in this part of the filament.

Recent simulation results have shown that a beam subjected to FRS undergoes many complex processes. In particular, pulse erosion of the front of the pulse is vital for generating a large amplitude plasma wave that serves to seed the interaction [15], [41]. As the laser beam propagates through the plasma wave, wavebreaking within the pulse as well as self-phase modulation causes the phase within the pulse to become incoherent. The bulk of the pulse is also susceptible to other instabilities (hosing, ponderomotive, ion motion) [5]. These effects reduce the effectiveness of the main part of this (relatively long) laser pulse in plasma wave generation. However, at the same time, the front end can become so deeply eroded that at relativistic laser intensities, the front edge generated plasma wave can be of the order of the wavebreaking limit. Indeed, we can estimate the amplitude of the plasma wave because on many shots, it is possible to observe the second harmonic of the plasma wave scattered into the diagnostic ($\omega_s = \omega_0 - 2\omega_p$). These are shots where the background from bremsstrahlung is low. At a large amplitude, the harmonic content of the plasma wave is an indicator of its nonlinearity, which is directly dependent on its amplitude. We estimate that the plasma wave amplitude is 40% (± 20) [26]. This is consistent with the wave amplitude observed in particle-in-cell (PIC) simulation [43] and is generally limited by beam loading of the electron plasma wave (EPW). The wakefield generated by a step function increase in intensity is given by $\delta n_e/n_0 = (1/2)a_0^4(1 + a_0^2)$, where the maximum normalized vector potential a_0 is related to the laser intensity I by $\Delta a_0 = (0.86 \cdot \lambda [\mu\text{m}] \cdot I^{1/2} [\times 10^{18} \text{ Wcm}^{-2}])$. This gives us an estimate for the intensity of the laser filament, which was observed for greater than 12 Rayleigh lengths from focus, at $8 \times 10^{17} \text{ Wcm}^{-2}$. Indeed, because the plasma wave amplitude is limited by beam loading effects, it is conceivable that the intensity in the filament is greater than this.

When the maximum possible vacuum intensity is reduced to this intensity (by reducing the laser energy by a factor of 6 from the maximum possible vacuum intensity of $5 \times 10^{18} \text{ Wcm}^{-2}$), the EPW scattered signal actually drops below the level observable by this diagnostic. Though, as we have already said, the vacuum focused intensity is never reached because of ionization-induced defocusing. Though other high-intensity effects, such as observation of intensity-dependent plasma frequency and half-harmonic Raman spectra, have been observed previously [10], spatially resolved Thomson scattering is the first positive indication of high-intensity effects within the filament of a channeling laser beam, and that these intensities persist over

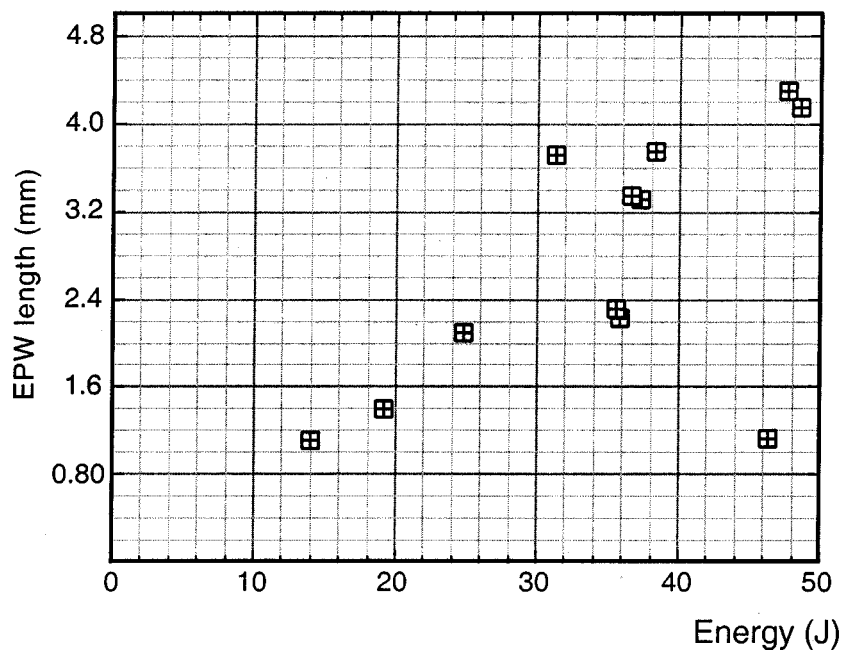


Fig. 10. Length of small-angle Thomson scattering image of an electron plasma wave as a function of incident laser energy in a 1-ps pulse, for a plasma of density $1.4 \times 10^{19} \text{ cm}^{-3}$.

$12\times$ the Rayleigh length is a clear verification of relativistic self focusing.

Also of interest in Fig. 9 is the spectrally broadband of light that appears over the whole spectrum but is spatially modulated. Because recombination light is not significant over the time range observed (≈ 1 ns), this light must be caused by laser-induced bremsstrahlung. The efficiency of bremsstrahlung emission is proportional to the number density of ions and electrons, but is very weakly dependent on temperature for plasma temperatures above 4 eV. For our plasma, just the above-threshold ionization heating of the first electron of helium should be well above this energy, so that the scattering observed is almost independent of temperature. Therefore, the large fluctuations of bremsstrahlung along the direction of propagation of the laser beam are the result of fluctuations in the number of scattering centers. This could be because of a decreasing number density caused by ponderomotive blow-out; however, the scattering from the plasma wave does not decrease where the bremsstrahlung intensity decreases. A severely cavitating channel is unlikely to support a large amplitude plasma wave; hence, it is unlikely that this is the reason for the changes in bremsstrahlung intensity. The number of scatterers is also dependent on the beam size, because a larger number are involved in the bremsstrahlung process, which is dependent only on photon number, not intensity. The varying intensity is, therefore, an indicator of varying spot size. As indicated in the figure, a variation of intensity from around 1500 counts to 350 counts per pixel corresponds to a doubling of the spot size. In fact, it is then remarkable that the spot size remains so constant over such long distances; e.g., for the first ≈ 1.5 mm at the front of the gas jet in this figure, the spot size would not be changing by more than 10%.

The length of the plasma wave scattered feature does not extend over the whole gas jet on all shots. Indeed, it is usually

smaller. Fig. 10 shows the variation of the Thomson scattered feature with intensity. Evidently, as the laser energy is increased, the channel length increases, though the shot-to-shot variation is high. A similar increase in length is also observed with increasing density (up to the maximum allowed for our gas jet). This suggests that the efficiency of channel creation is roughly proportional to P/P_{cr} .

E. Forward Raman Scattering

This interaction is characterized by its susceptibility to FRS. This is manifest in the modulation of the transmitted laser spectrum at multiples of the plasma frequency. Also characteristic is production of high fluxes of electrons ($>10^8$ in a $f60$ cone) that result from the transition to turbulence of the daughter EPW generated by the FRS. This chaotic behavior is termed wave-breaking, and it occurs when the EPW amplitude $\Delta n_e/n_0$ is close to unity, i.e., when charge sheets are able to overlap in the longitudinal wave, such that electrons from one oscillation period cross over to the next period and, thus, feel a large accelerating force rather than the returning force of their harmonic motion. This behavior is clear in the spectra of the transmitted light, in which the first satellite (shifted at ω_p from ω_0) becomes broad and modulated as its amplitude reaches close to that of the fundamental frequency light. Fig. 11 shows the number of electrons detected in energy channels between 23 and 29 MeV as a function of plasma frequency. Also plotted are the amplitudes of the anti-Stokes satellite versus the transmitted light at the fundamental frequency. As can be seen, the satellite height rises rapidly as ω_p (and, thus, density) is increased, until at a density close to $1 \times 10^{19} \text{ cm}^{-3}$ ($\omega_p/\omega_0 \approx 0.1$), it reaches close to unity. At this density, the electron signal at this energy increases even more rapidly, to a maximum of around 10^6 electrons/mega-electronvolts for some shots. This rapid increase in electron numbers corresponds to wavebreaking.

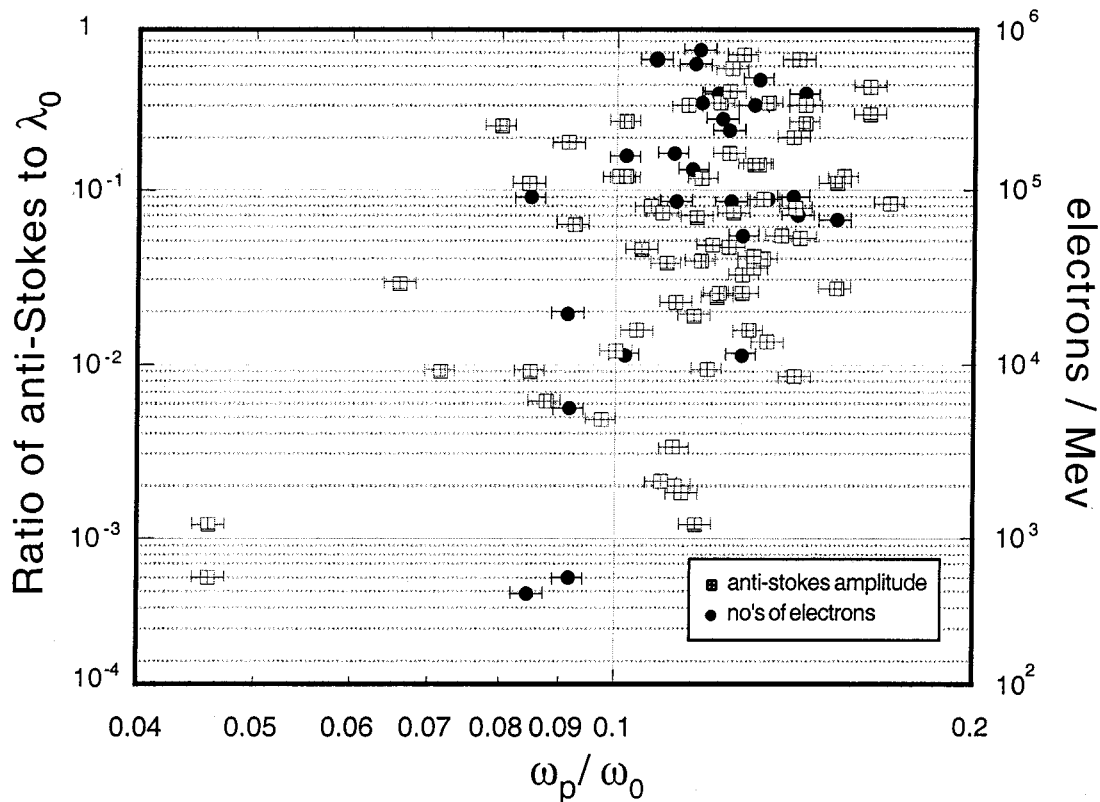


Fig. 11. Ratio of anti-Stokes to fundamental frequency of transmitted beam as a function of plasma frequency, and numbers of electrons detected in an $f60$ cone between 23 and 29 MeV as a function of plasma frequency, for shots with laser power in the range 22 to 30 TW.

Some electron kinetic energy spectra are shown in Fig. 12 for shots at the same laser power and plasma density, which exhibited different channel lengths in the image and Thomson scattering channels. The dephasing energy is given by $W_{\max} \approx 2\gamma_{\text{ph}}(1 + \epsilon\gamma_{\text{ph}})m_e c^2$ (valid in the limit $\epsilon\gamma_{\text{ph}} > 1$) [42]. In these shots, the Lorentz factor $\gamma_{\text{ph}} = 8.5$ ($n_e = 1.4 \times 10^{19} \text{ cm}^{-3}$), and as found previously, the EPW amplitude ($\epsilon = (\delta n_e/n_0)$) is measured to be 0.4. Hence, the expected maximum energy gain would be 55 MeV. As can be seen, the highest energy observed is 90 MeV. In fact, a further doubling of the density produces very little change in the spectrum observed, despite an almost $4\times$ reduction in the maximum expected energy gain. The extra acceleration is not caused by nonlinear steepening of the wake amplitude because then we would measure higher values of ϵ with our Thomson scattering diagnostic. Indeed, PIC simulations show that wake amplitudes never exceed our measured value because of beam loading effects [43]. These simulations also exhibit the same enhanced acceleration. The effect is attributed to the high current of electrons that are accelerated by the EPW. The leading part of the (micro) bunch of accelerated electrons can form a plasma wakefield in which to accelerate trailing electrons, so creating a staged acceleration process. However, this simple picture can be complicated by many other effects, such as self-generated focusing fields [44], relativistic effects [5], incoherent plasma dynamics [45], and a nonlinear group velocity of light in the plasma wave [46].

Also of note in Fig. 12 is that neither the electron energies nor, more surprisingly, the electron numbers increase with increasing channel length. The former is evidently a

result of the most energetic electrons being close to their (modified) dephasing energies, because the dephasing length $L_d = 2\gamma^2\lambda_p/\pi \approx 400 \mu\text{m}$ is less than the length of the channel. The number of electrons accelerated might be thought to increase with an increase in the amount of plasma over which the plasma wave grows. In fact, it decreases. Although very few shots are observed with the longest channel lengths, there can be many explanations as to why this happens; it could just be that the filaments are misaligned with our rather narrow electron spectrometer entrance and so results in decreased signal observation. Also, an increased channel length means the presence of longer lengths of transverse electric fields that could act to deflect many electrons. It seems at any rate that the number of trapped electrons within the filaments is not particularly great.

FRS is a four-wave process, because a downshifted Stokes line cannot directly couple to the pump laser and a seed relativistic plasma wave caused by the wavematching conditions. Hence, in FRS, the upshifted and downshifted Raman components should be created with equal amplitude. Fig. 13 shows the variation in intensity of the Stokes and anti-Stokes Raman satellite as a function of density. As can be clearly seen, this is not the case, especially at low densities ($\omega_p/\omega_0 < 0.08$), where the Stokes satellite is much greater in amplitude than is the anti-Stokes component. As density increases, the anti-Stokes component increases in amplitude relative to the Stokes component. Indeed, it appears as if the Stokes component is falling in amplitude. However, our collecting system is far from ideal for this measurement, because we use an Si-based CCD camera

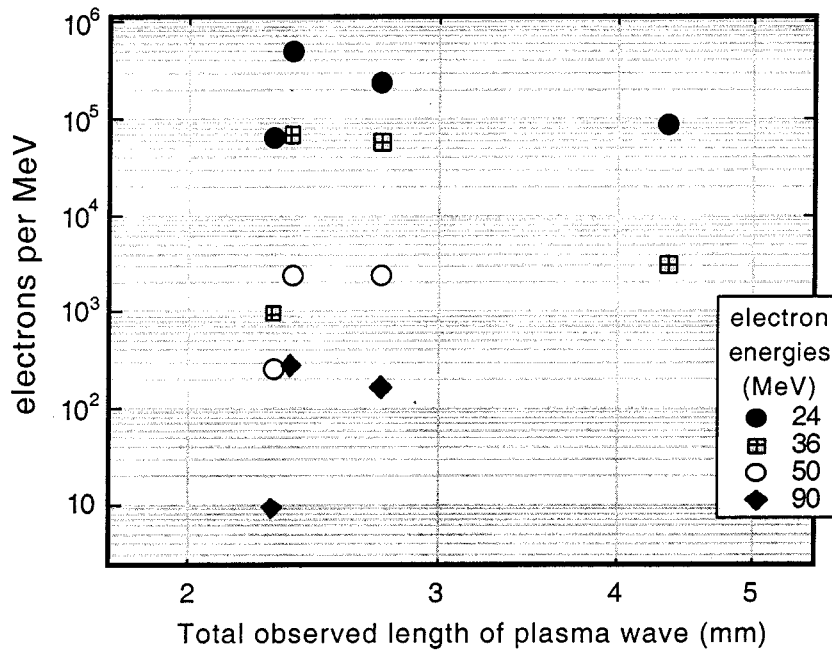


Fig. 12. Numbers of electrons accelerated to four given energies as a function of electron plasma wave length (as measured by small-angle Thomson scattering), on four shots with power between 25- and 30-TW beam in a plasma of density of $1.4 \times 10^{19} \text{ cm}^{-3}$.

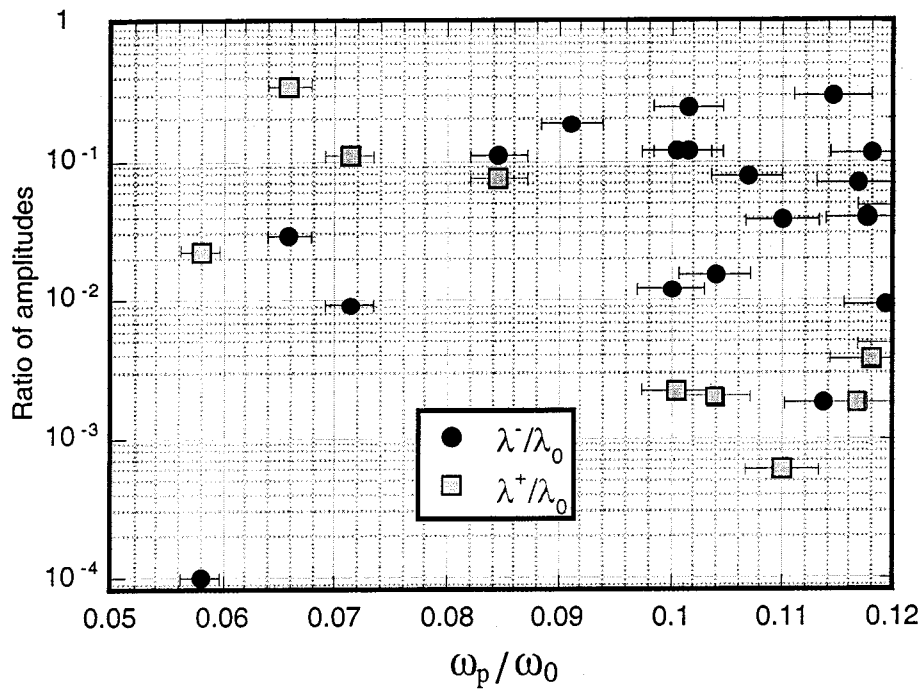


Fig. 13. Ratio of Stokes (λ^+) and anti-Stokes (λ^-) lines in the transmitted Raman spectra to the transmitted laser energy at λ_0 , plotted as a function of plasma frequency.

as the detector, which has a serious fall in sensitivity beyond $\approx 1100 \text{ nm}$, so that our detection system is almost blind to the Stokes satellite for densities greater than $1 \times 10^{19} \text{ cm}^{-3}$. These findings seem to be confirmed, though, when the detection is performed with a (bolometric) thermal imager with a sensitivity up to $\approx 2 \text{ }\mu\text{m}$. However, because of the low dynamic range of this detector and the associated large error, these data are not presented here. It seems clear then that the four-wave process is preceded by a three-wave process, which preferentially am-

plifies the Stoke satellite. A similar dependence with intensity is also observed, with the Stokes satellite greater in amplitude than the anti-Stokes at low laser powers, but with the anti-Stokes amplitude rising most rapidly until at high powers ($> 15 \text{ TW}$ for $n_e = 1.5 \times 10^{19} \text{ Wcm}^{-2}$), they are approximately equal in amplitude. Theoretical studies of FRS show that there are clear regimes for which either the three-wave, four-wave nonresonant (where both Stokes and anti-Stokes grow, but the former has a higher growth) or four-wave resonant (where Stokes and

anti-Stokes grow equally) are dominant. Indeed, as we increase intensity, the scattering evolves from three-wave to four-wave nonresonant to four-wave resonant, in that order [9], [47]. So the observed trend of larger Stokes leading to equal Stokes and anti-Stokes amplitude is as expected. However, with increasing density, the opposite should happen, because the plasma wave wavenumber decreases, so that the mismatch in wavenumber decreases. Hence, we would expect the Stokes and anti-Stokes to be more equal in amplitude with decreasing density, opposite to what is observed. The reason may well be because of the influence of Raman sidescatter. Three-wave processes are allowed off-axis; however, for the four-wave process, the amount of mismatch increases at angles away from direct forward scattering. Three-wave small-angle sidescatter also has a relatively high growth rate, and it can be amplified over as much length as direct forward scattering because of the large range of angles occupied by our laser beam because of the high f -number focusing optic ($\approx f4$). Because it can then propagate with the driver laser beam, it will be detected in the transmitted beam spectrum and can act as a supplementary seeding mechanism for four-wave FRS.

IV. CONCLUSION

The dynamics of a high-intensity short pulse laser propagating in an underdense plasma has been characterized through the simultaneous use of several different diagnostics. Importantly though, none of the reported high-intensity effects is observed if the laser beam has to propagate through nonionized gas before focus. This is because of ionization-induced refraction that prevents the laser beam from focusing as tightly as possible in vacuum. Hence, to observe high-intensity effects, it is necessary to focus the laser to the edge of a gas jet with a sharp gas–vacuum interface. Even in this case, the effect of ionization-induced refraction is still evident, in that it takes laser powers several times the theoretical value to observe effects such as relativistic self-focusing (though of course this is exacerbated by the far-from-ideal beam quality that such high-power systems possess).

The beam focused to high intensity at the edge of the jet is found to be susceptible to FRS. The growth of FRS increases rapidly with density but only weakly with intensity, as expected for FRS at relativistic intensities ($a_0 \sim 1$). At sufficiently high density, this can lead to the FRS satellites becoming comparable in amplitude to the fundamental frequency. This, correlated with the observation of a high flux of accelerated electrons ($>10^{11}$ for $E > 2$ MeV), indicates wavebreaking of the FRS's daughter relativistic plasma wave. Some electrons are found to be accelerated well above the dephasing energy, up to 94 MeV, suggesting that the accelerating plasma wave has been modified by beam-loading effects.

Images of the self-scattered light of the propagating beam orthogonal to the beam show signs of channeling away from focus. However, these are only apparently over any extended length for powers many times the critical power for relativistic self-focusing. At yet higher ratios of laser power to critical power, the beam breaks into more than just one filament. Spectral examination of this self-scattered light shows that it is mostly from cold

plasma and, hence, is indicative only of the interaction of light at low intensities escaping from the side or end of any self-guided channels. At the highest densities and intensities, stimulated Compton scattering is also observed at 90° to the laser propagation, but only close to the vacuum–gas interface. Hence, it is difficult to fully characterize a channeling laser beam through only self-scattered images.

High intensities within the guided channel can be directly ascertained through small-angle Thomson scattering of an orthogonal probe beam. This allows us to measure the plasma wave generated in the filament at the end of the gas jet away from focus. On some shots, it is found to be as great as at the start of the jet, which from simple wakefield theory suggest intensities of the order of 10^{18} Wcm $^{-2}$. That these channels are formed by relativistic self-focusing is supported by observing the fundamental of the self-scattered light, which often shows a red-shifting, consistent with the increasing refractive index caused by an intensity increase. Though schlieren images show density gradients are present after the laser beam passes, it is clear that the channel is not fully cavitating; otherwise, it would not be able to support a relativistic plasma wave. Though the length and direction of the filaments varies greatly shot to shot, the accelerated electron signal is not found to depend greatly on the channel length. Hence, the filaments contribute little to the electron acceleration process.

ACKNOWLEDGMENT

The authors would like to thank W. Mori and K.-C. Tzeng for helpful discussions and suggestions.

REFERENCES

- [1] M. Tabak, J. Hammer, M. E. Glinsky, W. L. Kruer, S. C. Wilks, J. Woodworth, E. M. Campbell, M. D. Perry, and R. J. Mason, "Ignition and high-gain with ultrapowerful lasers," *Phys. Plasmas*, vol. 1, p. 1626, 1994.
- [2] Z. H. Chang, A. Rundquist, H. W. Wang, M. M. Murnane, and H. C. Kapteyn, "Generation of coherent soft X rays at 2.7 nm using high harmonics," *Phys. Rev. Lett.*, vol. 79, p. 2967, 1997.
- [3] P. A. Norreys, M. Zepf, S. Moustazis, A. P. Fews, J. Zhang, P. Lee, M. Bakarezos, C. N. Danson, A. Dyson, P. Gibbon, P. Loukakos, D. Neely, F. N. Walsh, J. S. Wark, and A. E. Dangor, "Efficient extreme UV harmonics generated from picosecond laser-pulse interactions with solid targets," *Phys. Rev. Lett.*, vol. 76, p. 1832, 1996.
- [4] C. Spielmann, N. H. Burnett, S. Sartania, R. Koppitsch, M. Schnurer, C. Kan, M. Lenzner, P. Wobruschek, and F. Krausz, "Generation of coherent X-rays in the water window using 5-femtosecond laser pulses," *Science*, vol. 278, p. 661, 1997.
- [5] E. Esarey, P. Sprangle, J. Krall, and A. Ting, "Overview of plasma-based accelerator concepts," *IEEE Trans. Plasma Sci.*, vol. 24, p. 252, 1996.
- [6] S. Laroche, A. Talebpoor, and S. L. Chin, "Non-sequential multiple ionization of rare gas atoms in a Ti:Sapphire laser field," *J. Phys. B*, vol. 31, p. 1201, 1998.
- [7] M. V. Ammosov, N. B. Delone, and V. P. Krainov, "Tunnel ionization of complex atoms and atomic ions in an alternating electromagnetic field," *Sov. Phys. JETP*, vol. 64, p. 1191, 1987.
- [8] C. A. Coverdale, C. B. Darrow, C. D. Decker, W. B. Mori, K. C. Tzeng, K. A. Marsh, C. E. Clayton, and C. Joshi, "Propagation of intense sub-picosecond laser-pulses through underdense plasmas," *Phys. Rev. Lett.*, vol. 74, p. 4659, 1995.
- [9] W. B. Mori, C. D. Decker, D. E. Hinkel, and T. Katsouleas, "Raman forward scattering of short-pulse high-intensity lasers," *Phys. Rev. Lett.*, vol. 72, p. 1482, 1994.
- [10] A. Modena, Z. Najmudin, A. E. Dangor, C. E. Clayton, K. A. Marsh, C. Joshi, V. Malka, C. B. Darrow, and C. Danson, "Observation of Raman forward scattering and electron acceleration in the relativistic regime," *IEEE Trans. Plasma Sci.*, vol. 24, p. 289, 1996.

- [11] C. E. Max, J. Arons, and A. B. Langdon, "Self-modulation and self-focusing of electromagnetic waves in plasmas," *Phys. Rev. Lett.*, vol. 33, p. 209, 1974.
- [12] S. C. Wilks, W. L. Kruer, M. Tabak, and A. B. Langdon, "Absorption of ultra-intense laser-pulses," *Phys. Rev. Lett.*, vol. 69, p. 1383, 1992.
- [13] M. Zepf, M. Castrocolin, D. Chambers, S. G. Preston, J. S. Wark, J. Zhang, C. N. Danson, D. Neely, P. A. Norreys, A. E. Dangor, A. Dyson, P. Lee, A. P. Fews, P. Gibbon, S. Moustazis, and M. H. Key, "Measurements of the hole boring velocity from doppler-shifted harmonic emission from solid target," *Phys. Plasmas*, vol. 3, p. 3242, 1996.
- [14] A. E. Dangor, A. K. L. Dymoke-Bradshaw, A. Dyson, T. Garvey, I. Mitchell, A. J. Cole, C. N. Danson, C. B. Edward, and R. G. Evans, "Generation of uniform plasmas for beatwave experiments," *IEEE Trans. Plasma Sci.*, vol. PS15, p. 161, 1987.
- [15] T. M. Antonsen and P. Mora, "Self-focusing and Raman-scattering of laser-pulses in tenuous plasmas," *Phys. Rev. Lett.*, vol. 69, p. 2204, 1992.
- [16] C. D. Decker, W. B. Mori, T. Katsouleas, and D. E. Hinkel, "Spatial temporal theory of Raman forward scattering," *Phys. Plasmas*, vol. 3, p. 1360, 1996.
- [17] C. J. McKinstrie and E. J. Turano, "Spatiotemporal evolution of parametric instabilities driven by short laser pulses: Two-dimensional analysis," *Phys. Plasmas*, vol. 4, p. 3347, 1997.
- [18] B. Quesnel, P. Mora, J. C. Adam, S. Guerin, A. Heron, and G. Laval, "Electron parametric instabilities of ultraintense short laser pulses propagating in plasmas," *Phys. Rev. Lett.*, vol. 78, p. 2132, 1997.
- [19] A. Modena, Z. Najmudin, A. E. Dangor, C. E. Clayton, K. A. Marsh, C. Joshi, V. Malka, C. B. Darrow, C. Danson, D. Neely, and F. N. Walsh, "Electron acceleration from the breaking of relativistic plasma-waves," *Nature*, vol. 377, p. 606, 1995.
- [20] C. Joshi, T. Tajima, J. M. Dawson, H. A. Baldis, and N. A. Ebrahim, "Forward Raman instability and electron acceleration," *Phys. Rev. Lett.*, vol. 47, p. 1285, 1981.
- [21] W. B. Mori, "The physics of the nonlinear optics of plasmas at relativistic intensities for short-pulse lasers," *IEEE J. Quant. Electron.*, vol. 33, p. 1942, 1997.
- [22] A. J. Mackinnon, M. Borghesi, A. Iwase, M. W. Jones, G. J. Pert, S. Rae, K. Burnett, and O. Willi, "Quantitative study of the ionization-induced refraction of picosecond laser pulses in gas-jet targets," *Phys. Rev. Lett.*, vol. 76, p. 1473, 1996.
- [23] S. C. Rae, "Spectral blueshifting and spatial defocusing of intense laser-pulses in dense gases," *Opt. Commun.*, vol. 104, p. 330, 1994.
- [24] K. Krushelnick, A. Ting, C. I. Moore, H. R. Burris, E. Esarey, P. Sprangle, and M. Baine, "Plasma channel formation and guiding during high intensity short pulse laser plasma experiments," *Phys. Rev. Lett.*, vol. 78, p. 4047, 1997.
- [25] S. Y. Chen, G. S. Sarkisov, A. Maksimchuk, R. Wagner, and D. Umstadter, "Evolution of a plasma waveguide created during relativistic-ponderomotive self-channeling of an intense laser pulse," *Phys. Rev. Lett.*, vol. 80, p. 2610, 1998.
- [26] C. E. Clayton, K. C. Tzeng, D. Gordon, P. Muggli, W. B. Mori, C. Joshi, V. Malka, Z. Najmudin, A. Modena, D. Neely, and A. E. Dangor, "Plasma wave generation in a self-focused channel of a relativistically intense laser pulse," *Phys. Rev. Lett.*, vol. 81, p. 100, 1998.
- [27] P. Sprangle, C. M. Tang, and E. Esarey, "Relativistic self-focusing of short-pulse radiation beams in plasmas," *IEEE Trans. Plasma Sci.*, vol. 15, p. 145, 1987.
- [28] X. L. Chen and R. N. Sudan, "Necessary and sufficient conditions for self-focusing of short ultraintense laser-pulse in underdense plasma," *Phys. Rev. Lett.*, vol. 70, p. 2082, 1993.
- [29] C. N. Danson, J. Collier, D. Neely, L. J. Barzanti, A. Damerell, C. B. Edwards, M. H. R. Hutchinson, M. H. Key, P. A. Norreys, D. A. Pepler, I. N. Ross, P. F. Taday, W. T. Toner, M. Trentelman, F. N. Walsh, T. B. Winstone, and R. W. W. Wyatt, "Well characterized 10^{19} Wcm⁻² operation of VULCAN—An ultra-high power Nd:glass laser," *J. Mod. Opt.*, vol. 45, p. 1653, 1998.
- [30] R. Bruckner, "Etude de l'ionization laser de jets de gaz haute densite," Ph.D. dissertation, Universite d'Orleans, 1994.
- [31] V. Malka, A. Modena, Z. Najmudin, A. E. Dangor, C. E. Clayton, K. A. Marsh, C. Joshi, C. N. Danson, D. Neely, and F. N. Walsh, "Second harmonic generation and its interaction with relativistic plasma waves driven by forward Raman instability in underdense plasmas," *Phys. Plasmas*, vol. 4, p. 1127, 1997.
- [32] A. K. Lal, D. Gordon, K. Wharton, C. E. Clayton, K. A. Marsh, W. B. Mori, C. Joshi, M. J. Everett, and T. W. Johnston, "Spatio-temporal dynamics of the resonantly excited relativistic plasma wave driven by a CO₂ laser," *Phys. Plasmas*, vol. 4, p. 1434, 1997.
- [33] P. Gibbon, P. Monot, T. Auguste, and G. Mainfray, "Measurable signatures of relativistic self-focusing in underdense plasmas," *Phys. Plasmas*, vol. 2, p. 1305, 1995.
- [34] P. Sprangle, J. Krall, and E. Esarey, "Hose-modulation instability of laser-pulses in plasmas," *Phys. Rev. Lett.*, vol. 73, p. 3544, 1994.
- [35] G. Shvets and J. S. Wurtele, "Instabilities of short-pulse laser propagation through plasma channels," *Phys. Rev. Lett.*, vol. 73, p. 3540, 1994.
- [36] F. Vidal and T. W. Johnston, "Electromagnetic beam breakup: Multiple filaments, single beam equilibria, and radiation," *Phys. Rev. Lett.*, vol. 77, p. 4852, 1996.
- [37] Z. Najmudin, K. Krushelnick, E. L. Clark, M. Salvati, M. I. K. Santala, M. Tatarakis, A. E. Dangor, V. Malka, D. Neely, R. Allott, and C. Danson, "Hosing, sausageing, filamentation and sidescatter of a high-intensity short-pulse laser in an under-dense plasma," presented at the IFSA, Bordeaux, France, 1999.
- [38] T. M. Antonsen and Z. Bian, "Ionization induced scattering of short intense laser pulses," *Phys. Rev. Lett.*, vol. 82, p. 3617, 1998.
- [39] M. Ciarrocca, J. P. Marangos, D. D. Burgess, M. H. R. Hutchinson, R. A. Smith, S. C. Rae, and K. Burnett, "Spectral and spatial modifications to an intense 1 μ m laser-pulse interacting with a dense argon gas," *Opt. Commun.*, vol. 110, p. 425, 1994.
- [40] K. C. Tzeng and M. W. B. Mori, "Suppression of electron ponderomotive blowout and relativistic self-focusing by the occurrence of Raman scattering and plasma heating," *Phys. Rev. Lett.*, vol. 81, p. 104, 1998.
- [41] C. D. Decker, W. B. Mori, K. C. Tzeng, and T. Katsouleas, "Evolution of ultra-intense, short-pulse lasers in underdense plasmas," *Phys. Plasmas*, vol. 3, p. 2047, 1996.
- [42] D. Gordon, K. C. Tzeng, C. E. Clayton, A. E. Dangor, V. Malka, K. A. Marsh, A. Modena, W. B. Mori, P. Muggli, Z. Najmudin, D. Neely, C. N. Danson, and C. Joshi, "Observation of electron energies beyond the linear dephasing limit from a laser-excited relativistic plasma wave," *Phys. Rev. Lett.*, vol. 80, p. 2133, 1998.
- [43] K. C. Tzeng, W. B. Mori, and T. Katsouleas, "Electron beam characteristics from laser-driven wave breaking," *Phys. Rev. Lett.*, vol. 79, p. 5258, 1997.
- [44] L. Gorbunov, P. Mora, and T. M. Antonsen, "Magnetic field of a plasma wake driven by a laser pulse," *Phys. Rev. Lett.*, vol. 76, p. 2495, 1996.
- [45] D. W. Forslund, J. M. Kindel, W. B. Mori, C. Joshi, and J. M. Dawson, "2-dimensional simulations of single-frequency and beat-wave laser-plasma heating," *Phys. Rev. Lett.*, vol. 54, p. 558, 1985.
- [46] C. D. Decker and W. B. Mori, "Group-velocity of large-amplitude electromagnetic-waves in a plasma," *Phys. Rev. Lett.*, vol. 72, p. 490, 1994.
- [47] S. Guerin, G. Laval, P. Mora, J. C. Adam, A. Heron, and A. Bendib, "Modulational and Raman instabilities in the relativistic regime," *Phys. Plasmas*, vol. 2, p. 2807, 1995.
- [48] V. Malka, C. Coulaud, J. P. Geindre, V. Lopez, Z. Najmudin, D. Neely, and F. Amiranoff, "Characterization of neutral density profile in a wide range of pressure of cylindrical pulsed gas jet," *Rev. Sci.*, vol. 71, p. 2329, 2000.

Z. Najmudin, photograph and biography not available at the time of publication.

A. E. Dangor, photograph and biography not available at the time of publication.

A. Modena, photograph and biography not available at the time of publication.

M. R. Salvati, photograph and biography not available at the time of publication.

C. E. Clayton, photograph and biography not available at the time of publication.

C. N. Danson, photograph and biography not available at the time of publication.

Daniel F. Gordon, received the B.S., M.S., and Ph.D. degrees in electrical engineering from the University of California, Los Angeles, in 1991, 1995, and 1999, respectively.

He is currently a National Research Council research associate at the Naval Research Laboratory, Washington, DC. His research interests are in high intensity, short pulse, laser-plasma interactions, plasma based accelerators, and computer modeling.

C. Joshi (M'83–SM'88–F'93), photograph and biography not available at the time of publication.

K. A. Marsh, photograph and biography not available at the time of publication.

V. Malka, photograph and biography not available at the time of publication.



Patrick Muggli received the B.S. and Ph.D. degrees from the Centre de Recherche en Physique des Plasmas, Ecole Polytechnique Fédérale de Lausanne, Switzerland, in the fields of plasma physics and high-power microwave sources.

He was a Swiss National Science Foundation post-doctoral fellow at the Electrical Engineering Department of the University of California, Los Angeles. He worked on frequency upshifting of electromagnetic radiation using plasmas, and on photoemission processes. He joined the University of Southern California (USC), Los Angeles, and his research topics include all aspects of plasma-based radiation sources, and plasma-based particle accelerators. He is currently an Assistant Research Professor at USC.

Dr. Muggli is the USC representative to the Coalition for Plasma Science.

D. Neely, photograph and biography not available at the time of publication.

F. N. Walsh, photograph and biography not available at the time of publication.